One-Step "Green" Synthesis of Pd Nanoparticles of Controlled Size and Their Catalytic Activity for Trichloroethene Hydrodechlorination

ARTICLE *in* INDUSTRIAL & ENGINEERING CHEMISTRY RESEARCH · JUNE 2009

Impact Factor: 2.59 · DOI: 10.1021/ie801962f

4 AUTHORS, INCLUDING:

Feng he
Zhejiang University of Technology
27 PUBLICATIONS **1,573** CITATIONS
SEE PROFILE

Juncheng Liu
Alto Products Corporation
47 PUBLICATIONS **1,469** CITATIONS
SEE PROFILE

Dongye Zhao
Auburn University
114 PUBLICATIONS **3,364** CITATIONS
SEE PROFILE

One-Step "Green" Synthesis of Pd Nanoparticles of Controlled Size and Their Catalytic Activity for Trichloroethene Hydrodechlorination

Feng He,[†] Juncheng Liu,[‡] Christopher B. Roberts,[‡] and Dongye Zhao*,[†]

Environmental Engineering Program, Department of Civil Engineering, Auburn University, Auburn, Alabama 36849, and Department of Chemical Engineering, Auburn University, Auburn, Alabama 36849

We present here a straightforward, one-step "green" approach for preparing Pd nanoparticles of controlled size and size distribution. The new catalysts were synthesized using a low-cost, biocompatible cellulose, sodium carboxymethyl cellulose (CMC), as a stabilizer and ascorbic acid as a reducing agent at temperatures ranging from 22 to 95 °C. The mean size and polydispersivity (expressed as standard deviation, SD) of the Pd nanoparticles was exponentially reduced by increasing the preparation temperature from 22 to 95 °C. At 95 °C, nearly monodisperse Pd nanoparticles were obtained with a mean diameter of 3.6 nm (SD = 0.5 nm). The Pd nanoparticles exhibited high catalytic reactivity when tested for hydrodechlorination of trichloroethene in the presence of H_2. The observed pseudofirst-order reaction rate constant, k_{obs}, was up to 692 L g^{-1} min^{-1}, which is comparable to the Pd nanoparticles synthesized per the conventional borohydride reduction method. This new approach not only offers a simple way to manipulate particle size and size distribution but also eliminates the need of borohydride, which is much more costly and less environmentally friendly than the ascorbic acid used in this work.

Introduction

Metal nanoparticles are of great importance because of their size-dependent material properties and the potential applications in various emerging areas of nanoscience and technology.[1,2] In recent years, with the rapid development of various new nanomaterials, the environmental concerns pertaining to the synthesis and environmental impacts of synthetic nanoparticles are also mounting. To ensure future sustainable development and applications of nanotechnologies, it is essential to implement the principles of "green" chemistry in every stage and aspect of the technology development from material manufacturing to the environmental fate of the nanomaterials including metal nanoparticles.[3−5] To this end, it is essential to develop environmentally more sound approaches for fabricating novel nanoparticles, where the uses of environmentally harmful chemicals and the associated environmental risks should be minimized.

Metal nanoparticles have shown great promise to improve conventional practices in environmental remediation. For example, the development of soil-dispersible zerovalent iron (ZVI) nanoparticles has led to an in situ remediation technology for degrading chlorinated solvents in soils and groundwater, which can potentially cut down the cleanup cost by as much as 90%.[6−10] Associated with the much greater specific surface area as well as the size-dependent catalytic activity, various metal catalysts have been shown to offer some unprecedented properties when used for degrading various environmentally important contaminants. For instance, nanoscale Pd nanoparticles, developed by our group using borohydride as a reducing agent, showed 296 times greater reactivity than a commercial powder Pd/Al_2O_3, when used for dechlorination of trichloroethene (TCE).[11] The catalytic activity of the Pd nanoparticles in terms of surface-area normalized reaction rate was found to increase with decreasing particle size (from 2.4 to 4.7 nm), which was attributed to the increase of the fraction of active edge and vertex sites as the particle size gets smaller.[11,12] Liou et al. evaluated the reactivity of resin-copper nanoparticles for carbon tetrachloride degradation and observed similar results.[13]

Conventionally, metal nanoparticles are prepared by reducing metal ions in solutions. Typically, strong reducing agents such as sodium borohydride or hydrazine are employed. For instance, our group synthesized a class of Pd nanoparticles using borohydride as the reducing agent with a carboxymethyl cellulose (CMC) as a stabilizer.[11] However, because of its highly reactive properties, borohydride or hydrazine poses great risks to the environment and human health. Other drawbacks of these strong reducing agents are pollution problems associated with manufacturing the chemicals and the harmful byproduct from the particle fabrication. Mild, and often more environmentally friendly, reducing agents such as glucose and ascorbic acid would overcome these shortcomings. However, the reduction of metal salts using these agents is either thermodynamically unfavorable or kinetically too slow to form the desired nanoparticles. For example, these weak reducing agents cannot reduce Fe^{2+} to obtain zerovalent iron (ZVI) nanoparticles. Although Pd nanoparticles were prepared at room temperature by reducing Pd^{2+} with ascorbic acid in the presence of a cationic surfactant cetyltrimethylammonium bromide (CTAB), the particles were found to be highly polydisperse in both size (ranging from 15 nm to >100 nm) and shape (from spheres to rods and large aggregates).[14] To date, there has been lacking a "green" and effective one-step approach to synthesize Pd nanoparticles of controlled size and size distribution.

Chlorinated solvents such as tetrachloroethene (PCE) and TCE are among the most detected organic contaminants in U.S. groundwater and soil.[6−10] For example, TCE has been detected in at least 852 of the 1 430 National Priorities List (NPL) sites.[15] Exposure to PCE or TCE has been associated with malfunction of the nerve system, liver and lung damage, abnormal heartbeat, coma, and even death.[14] One promising technology to remediate TCE contaminated groundwater is using Pd particles to catalyze the hydrodechlorination of TCE by H_2 to readily biodegradable ethane.[11,16,17] However, the practical feasibility of this technology is largely limited by the high cost of Pd catalyst (the 2008

* Corresponding author: zhaodon@auburn.edu.
[†] Environmental Engineering Program, Department of Civil Engineering.
[‡] Department of Chemical Engineering.

10.1021/ie801962f CCC: $40.75
Published on Web 06/19/2009

commercial price of Pd is U.S. $450/oz) and low catalytic reactivity. To improve the cost-effectiveness and to promote the concept of "green" synthesis, a number of strategies can be exercised, including: (1) improve the particle preparation recipe and use cheaper and biocompatible raw chemicals, (2) improve the surface catalytic activity, and (3) increase the specific surface area of the Pd particles. Because nanoscale particles offer much greater specific surface area and because of the size-dependent properties of nanoparticles, developing a new class of monodisperse Pd nanoparticles is expected to greatly enhance the effectiveness of the catalytic applications of Pd particles.

The objectives of this study were to (1) develop a simple one-step and "green" approach to synthesize Pd nanoparticles of controlled size and size distribution using ascorbic acid as reducing agent and CMC as stabilizer and (2) test the catalytic activity of the nanoparticles by measuring the hydrodechlorination of TCE with H_2. In this work, special attention was placed to incorporating green chemistry principles into controlled fabrication of highly stable Pd nanoparticles and their potential environmental applications.

Experimental Section

Materials. $Na_2PdCl_4 \cdot 3H2O$ was purchased from Strem Chemicals (Newburyport, MA, U.S.A.). Carboxymethyl cellulose (CMC) sodium salt (average MW: ~90 000) and TCE of spectrophotometric grade (>99%) were obtained from Sigma-Aldrich (St. Louis, MO, U.S.A.). L-Ascorbic acid and hexane (pesticide grade) were obtained from Fisher Scientific (Fair Lawn, NJ, U.S.A.).

Aqueous-Phase Synthesis of Pd Nanoparticles. The Pd nanoparticles were synthesized in a one-step reduction process in an aqueous solution. To probe the temperature effect on the particle-size distribution, the particles were synthesized at 22, 50, 80, and 95 °C. In a typical preparation, a 1 mL aliquot of a 0.05 M $Na_2PdCl_4 \cdot 3H_2O$ aqueous solution was added and well-mixed into 250 mL of an aqueous solution containing 0.15 wt % of CMC. The mixture was then placed in a heating magnetic stirrer and kept at a desired temperature (22, 50, and 80, and 95 °C). Subsequently, ~3.5 mL of a 0.05 M ascorbic acid aqueous solution was added to the Pd-CMC solution under constant stirring (which gave a pH of ~3) and at the preset temperatures for 5 min. The reactor was then air-cooled to ambient temperature (22 °C) and aged (with gentle stirring) for 24 h before the suspension was used for particle characterization and subsequent TCE hydrodechlorination tests. The final Pd concentration in the aqueous suspension was 0.2 mM or 21 mg/L.

Particle Characterization. The morphology and size distribution of the Pd nanoparticles were determined with a Zeiss EM 10 TEM (Carl Zeiss, Oberkochen, Germany) at an operating voltage of 60 kV. Samples of the air-dried Pd nanoparticles were prepared by placing three droplets of a Pd nanoparticle suspension onto a copper grid and subsequently air-drying the samples overnight under ambient conditions.

X-ray diffraction (XRD) patterns were collected with a Rigaku Miniflex powder X-ray diffractometer with Cu Kα (λ = 1.540 Å) radiation. For XRD analyses, solid samples of the CMC-Pd nanoparticles were separated from the aqueous suspension by centrifugation at 4185 g with ethanol as an antisolvent and then dried overnight in an oven at 80 °C.

TCE Hydrodechlorination. Batch experiments were conducted using 127 mL serum bottles capped with Teflon septa. Typically, 4.5 mL of a Pd nanoparticle suspension (prepared at each of the preset temperatures) was initially mixed with 85 mL of deionized water under stirring, which resulted in a Pd nanoparticle concentration of 1.06 mg/L. Then, the reactor was sparged with hydrogen gas for 20 min to displace dissolved oxygen (DO) in the solution and to fill the headspace with H_2 (1 atm), i.e., the solution was presaturated with H_2. After the reactor was capped, the catalytic dechlorination was initiated by spiking 25 μL of a TCE stock solution (179 g/L TCE in methanol) into the reactor suspension, which resulted in an initial total TCE concentration of 50 mg/L. The reaction was conducted at 22 ± 1 °C and pH ~4 under constant magnetic stirring, and was followed for about 10 min. At constant time intervals (2 min), 0.1 mL of each aqueous sample including the suspended Pd nanoparticles was withdrawn using a 100 μL gas-tight syringe. Then, the samples were transferred into 2 mL gas chromatograph (GC) vials, each of which contained 1 mL of hexane to extract residual TCE or any possible hydrophobic byproducts. Upon phase separation, TCE and the possible chlorinated reaction intermediates were analyzed using an HP 6890 GC equipped with an electron capture detector (ECD). The GC was programmed as follows: The initial oven temperature was set at 35 °C for 8 min and ramped to 60 at 5 °C/min, then to 200 at 17 °C/min, and then to 250 at 50 °C/min. Injector and detector temperatures were both at 250 °C. All batch experiments were duplicated to ensure data quality.

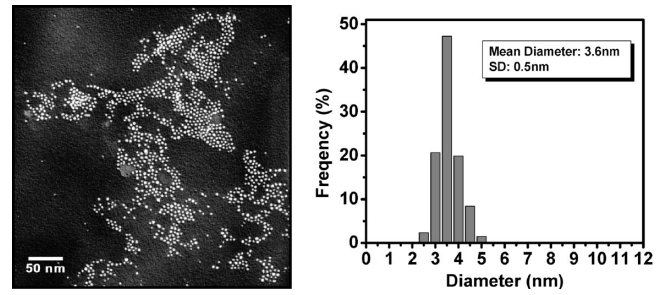

Figure 1. Representative TEM image of CMC-stabilized Pd nanoparticles synthesized at 95 °C in an aqueous system, and the corresponding particle-size distribution histogram. Pd and CMC concentration were 0.2 mM and 0.15 wt %, respectively.

Results and Discussion

Characterization of CMC-Pd Nanoparticles. The brief 5 min heating played a critical role in the synthesis of the Pd nanoparticles, i.e., reduction of Pd^{2+} to Pd^0 with ascorbic acid. At 95 °C, the CMC-Pd^{2+} solution turned to transparent dark brown as soon as ascorbic acid was added, indicating rapid reduction of Pd^{2+} and formation of fine Pd nanoparticles. In contrast, at the ambient temperature (22 °C), the solution slowly (~2 min) turned to turbid brown, suggesting formation of larger colloidal Pd particles. Figure S1 (Supporting Information) presents a visual comparison of the suspension appearances obtained at various temperatures. In contrast, Pd nanoparticles synthesized in the absence of CMC aggregated rapidly and precipitated in less than 1 day, suggesting the important role of CMC as a stabilizer.

Figure 1 shows a typical transmission electron microscope (TEM) image of the CMC-stabilized Pd nanoparticles synthesized at 95 °C and the size-distribution histogram. On the basis of this TEM image of 823 nanoparticles, a mean diameter of 3.6 nm was estimated with a standard deviation (SD) of 0.5 nm, indicating that the nanoparticles are nearly monodisperse (Note: the histogram was highly reproducible when more TEM images were used). To further determine the particle size and characterize the crystalline structure of the Pd nanoparticles,

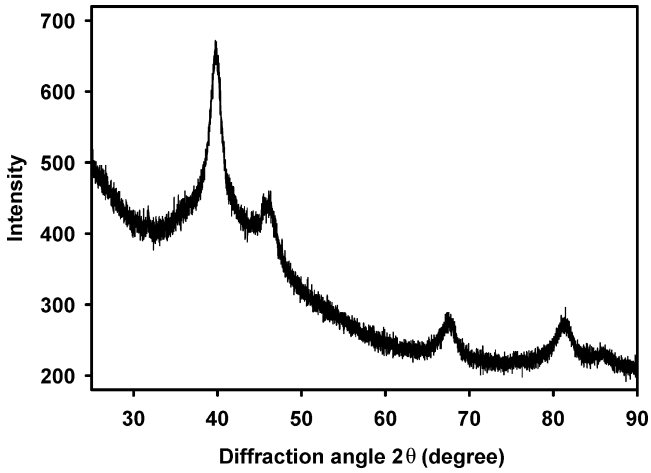

Figure 2. XRD pattern of CMC-Pd nanoparticles synthesized at 95 °C.

XRD analysis on the dried CMC-Pd particles was performed. Figure 2 shows the obtained XRD pattern. Five peaks were observed in the XRD pattern at around 40°, 46°, 68°, 82°, and 86°, respectively. These peaks correspond to, respectively, the {111}, {200}, {220}, {311}, and {222} planes of a face-centered-cubic (fcc) lattice, indicating the fcc structure of the CMC-Pd nanoparticles. Per the Scherrer equation[18] and on the basis of the XRD data in Figure 2, the mean diameter of the CMC-Pd nanoparticles is determined to be 4.4 nm, which is a bit greater than the TEM-based particle size. The discrepancy could result from many factors such as sample preparation and effect of the stabilizers as well as the inherent errors of these two methods. The CMC-stabilized Pd nanoparticles remained highly stable in the aqueous solution and did not show any precipitation when stored under ambient conditions for 9 months.

The Pd synthesis approach employs environmentally more friendly stabilizers and reducing agents. Cellulose is one of the most abundant polysaccharides, which belong to the most abundant natural and renewable biopolymers. Cellulose consists of anhydroglucose subunits, which are joined by so-called *beta* linkage to form a linear chain structure. Although it is linear and nominally thermoplastic, native cellulose is not water-soluble.[19] However, cellulose can be easily converted to water-soluble derivatives such as CMC with desired features.[19] CMC has been commonly used in food processing.[20] Ascorbic acid is a water-soluble sugar acid with antioxidant properties. The L-enantiomer of ascorbic acid is commonly known as vitamin C. Compared to borohydride (the classical reducing agent for preparing metallic particles), ascorbic acid is much "greener" in terms of biocompatibility, toxicity (borohydride is considered toxic according to material safety data sheet (MSDS) data), application safety (e.g., large amounts of H_2 can be generated from reactions between metal ions and borohydride), chemical manufacturing, and generation of harmful byproduct (e.g., borates are produced with borohydride reduction).

Effects of Preparation Temperature on Particle Size and Size Distribution. Figure 3 shows representative TEM images of Pd nanoparticles synthesized at 22, 50, and 80 °C. Evidently, the particle size and size distribution are strongly dependent on the synthesizing temperature. The nanoparticles synthesized at 22 °C displayed a mean diameter of 55 nm with a SD of 36 nm. During the particle preparation, the color of the CMC-Pd^{2+} solution started turning turbid brown ~2 min after the addition of ascorbic acid, indicating the slow reduction of Pd^{2+} and ineffective nucleation of the Pd atoms at ambient temperature. Increasing the initial synthesis temperature from 22 to 50 °C reduced the nanoparticle size to 26 nm (by a factor of 2.1) and greatly narrowed the size distribution (SD = 8.0 nm). The color of the CMC-Pd^{2+} solution changed in a few seconds. Further increasing the temperature to 80 °C resulted in smaller Pd nanoparticles of 6.5 nm with a narrower SD of 1.9 nm. The color of the CMC-Pd^{2+} solution changed to clear brown immediately with the addition of ascorbic acid at temperature 80 °C and higher. Figure 4 plots the mean size and the associated SD of the Pd nanoparticles as a function of synthesis temperature. It appears that the diameter and SD of Pd nanoparticles exponentially decrease as synthesis temperature is raised from 20 to 95 °C. Note that, in all cases, the mild heating lasted for only 5 min, suggesting that the reduction of Pd^{2+} ions at above-ambient temperature was a relatively fast process and, more importantly, the particle formation and the nature of the nanoparticles are governed by the initial (< 1 minute) synthesizing conditions (especially temperature and reaction kinetics in this case).

The redox reactions of Pd^{2+} and ascorbic acid during the particle synthesis can be described by eqs 1 and 2:

$$Pd^{2+} + 2e^- \rightarrow Pd^0 \quad E^0 = 0.951\ V\ ^{21} \tag{1}$$

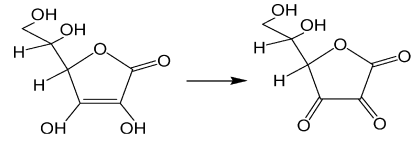

$$E^0 = 0.08\ V^{21} \tag{2}$$

Because fast initial nucleation or clustering of metal atoms is critical to the production of stable nuclei and subsequently smaller metal nanoparticles, controlled nucleation is a critical step in governing the formation and size distribution of metal nanoparticles.[22,23] Compared to the reduction of Pd^{2+} by borohydride (E^0 for BH_4^-/B is −1.31 V),[24] although the reduction of Pd^{2+} by ascorbic acid is thermodynamically favorable, it is kinetically much slower at ambient temperature, which results in inefficient nucleation of Pd atoms and the formation of big Pd clusters. The slower reduction of Pd^{2+} by ascorbic acid is evident from the fact that it took ~2 min before Pd particles were observed at room temperature, while the reduction of Pd^{2+} by borohydride was immediate. However, as the redox reaction can be accelerated by increasing temperature (e.g., it is generally assumed that the reaction rate doubles for every 10 °C increment), and because fast reduction of Pd^{2+} promotes fast nucleation of the resultant Pd atoms, the particle formation and particle size can be controlled by manipulating the synthesis temperature. Such temperature-facilitated particle control is less effective for strong reducing agents such as borohydride, which reduces the metal ions much more rapidly even at ambient temperatures.

The brief 5 min heating can also affect the subsequent particle nucleation and growth. The increased initial reduction rate at elevated temperatures results in a greater extent of supersaturation of Pd atoms and formation of more seed nuclei.[25] Consequently, more and smaller nanoparticles are produced.[25] Rapid initial nucleation also favors size uniformity because all seed particles are generated at about the same time and size and grow concurrently under the same conditions. The heating also greatly enhances Ostwald ripening during the first 5 min and beyond. Note that, although heating was ceased after the initial 5 min, the reactor was not quenched but rather allowed to cool gradually under room temperature. Thus, the residual heat continued to affect the particle growth, which promotes

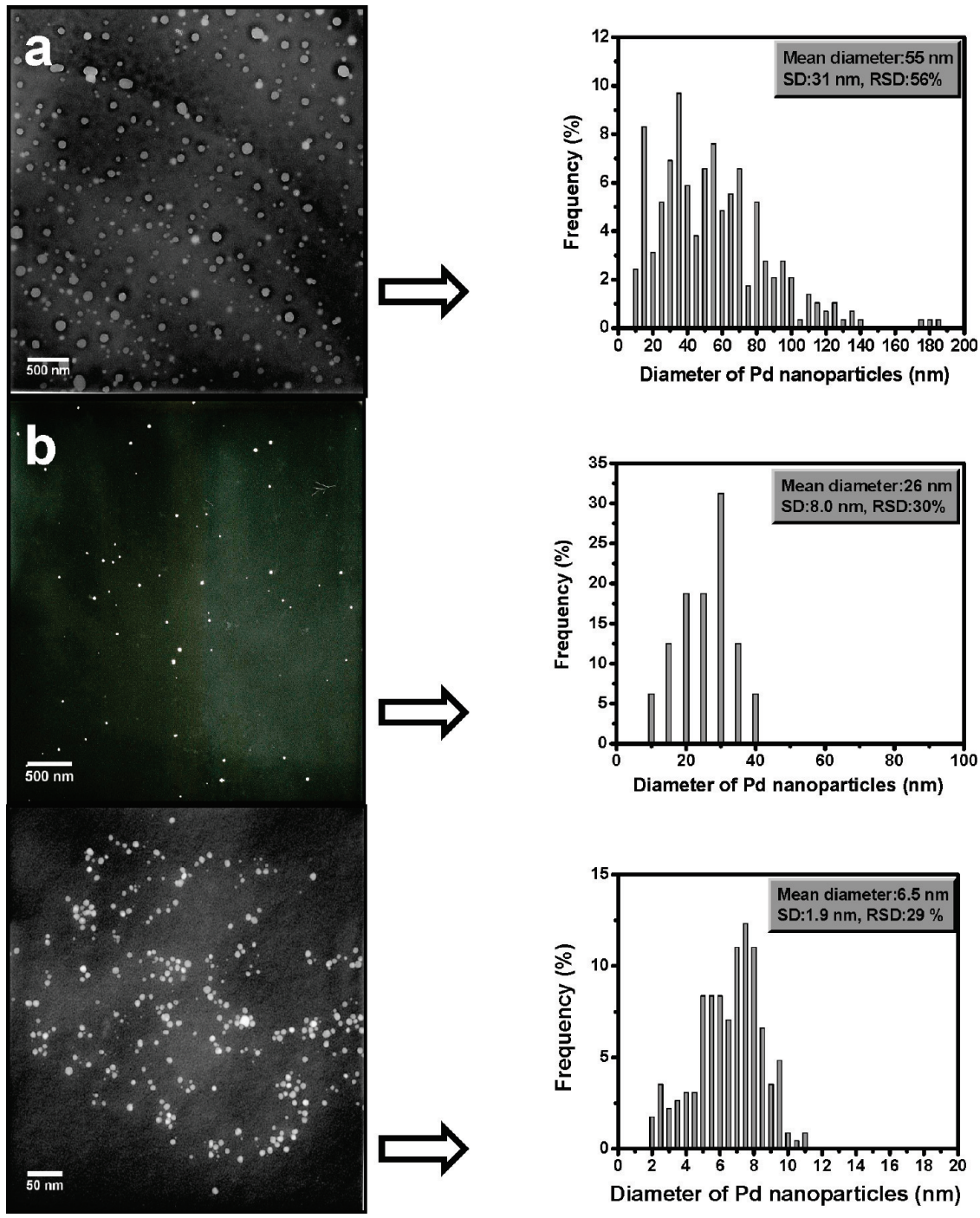

Figure 3. TEM images of Pd nanoparticles synthesized at (a) 22 °C, (b) 50 °C, and (c) 80 °C, along with the histograms of these Pd nanoparticles.

diffusion of the growth species on one hand, and dissolves more smaller particles on the other. As a result, the size distribution is greatly narrowed at elevated temperatures. Extended heating time was avoided in this work because overpromoting Ostwald ripening would favor survival of larger particles and end up with larger particle sizes. However, the heating scheme can be further refined to optimize the results. Furthermore, heating during particle growth disfavors diffusion-controlled growth, which can lead to more polydisperse particles.

Catalytic Activity of CMC-Pd Nanoparticles Synthesized at Various Temperatures. The synthesized Pd nanoparticles were tested in catalyzing the hydrodechlorination of TCE by H_2. As shown in Figure 5, 100% of TCE was degraded within 6 min by H_2 in the presence of the Pd nanoparticles synthesized at 95 °C, compared to 52%, 70%, and 87% of TCE degradation with the nanoparticles synthesized at 22, 50, and 80 °C, respectively. Our control tests (data not shown) indicated that the presence of only CMC-Pd or H_2 and CMC-Pd/ascorbic acid did not degrade any TCE. For all cases, a linear relation of $\ln(C/C_0)$ versus time was observed (Figure 5b), indicating the degradation of TCE by H_2 can be interpreted by the pseudofirst-order rate law with respect to TCE concentration,

$$-\frac{\mathrm{d[TCE]}}{\mathrm{d}t} = k_{\mathrm{app}} \cdot [\mathrm{TCE}] = k_{\mathrm{obs}} \cdot [\mathrm{Pd}] \cdot [\mathrm{TCE}] = k_{\mathrm{SA}} \alpha_{\mathrm{s}} [\mathrm{Pd}][\mathrm{TCE}] \quad (3)$$

where the k_{app} is the apparent reaction rate constant, [Pd] is the concentration of Pd nanoparticles, and [TCE] is the concentration of TCE during the reaction. The observed reaction rate

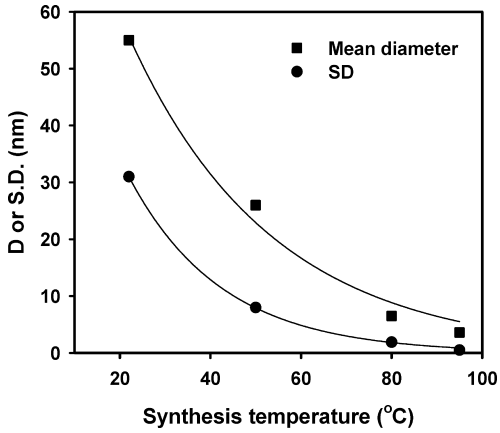

Figure 4. Effect of synthesis temperature on the size (mean diameter D) and size distribution (standard deviation, SD) of CMC-stabilized Pd nanoparticles.

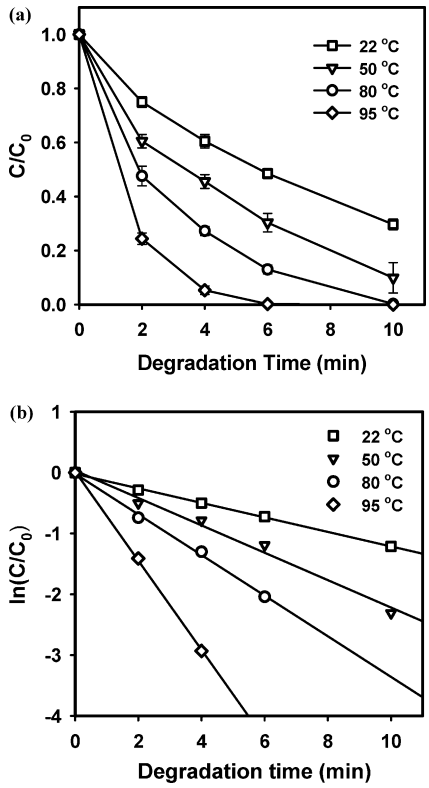

Figure 5. (a) Hydrodechlorination of TCE catalyzed by CMC-Pd nanoparticles synthesized at different temperatures under ambient conditions. Initial TCE concentration = 50 mg L^{-1}; Pd nanoparticles mass concentration = 1.06 mg L^{-1}. (b) Plot of $\ln(C/C_0)$ versus time showing the pseudofirst-order degradation of TCE.

constant (k_{obs}) is then derived by normalizing k_{app} to the Pd catalyst concentration (1.06 mg/L). The surface-area based rate constant (k_{SA}) was obtained by further normalizing the rate constant to the specific surface area (α_s).

The results are summarized in Table 1. It is worth pointing out that H_2 in the degradation system far exceeded the stoichiometric demand for complete TCE transformation. As a result, the H_2 concentration in the suspension phase remained essentially constant during the reaction.

On the basis of the k_{obs} values in Table 1, the overall catalytic activity of Pd nanoparticles follows the order of CMC-Pd (95 °C, 3.6 nm) > CMC-Pd (80 °C, 6.5 nm) > CMC-Pd (50 °C, 26 nm) > CMC-Pd (22 °C, 55 nm). This observation is consistent with the fact that smaller nanoparticles offer greater specific surface area and, thus, greater reactivity for TCE hydrodechlorination. When the synthesis temperature increased from 22 to 95 °C, the corresponding k_{obs} value increased from 112 to 692 L g^{-1} min^{-1}, a factor of 6.2. In all cases, halogenated intermediates, such as vinyl chloride (VC) and dichloroethenes (DCEs), were not detected during the course of hydrodechlorination of TCE, suggesting a complete dechlorination of the environmentally deleterious TCE. When the rate constants are normalized to specific surface area, the k_{SA} values decreased by a factor of 3.9 when temperature was increased from 22 to 95 °C, where k_{SA} remained about the same above 80 °C.

Table 1. Size, Number of Atoms, and Surface Area of CMC-Pd Nanoparticles Synthesized at Different Temperatures, and TCE Degradation Rate Constants and Initial Turnover Frequency (TOF)

	Pd nanoparticles synthesized at various temperatures with the same total concentration of Pd (0.2 mM) and CMC (0.15 wt %)			
	22 °C	50 °C	80 °C	95 °C
size (nm)	55 ± 31	26 ± 8.0	6.5 ± 1.9	3.6 ± 0.5
no. of atoms/particle	3 199 064	326 659	4 183	568
surface atoms/particle	96 312	20 797	1 058	254
D_{Pd}	0.03	0.06	0.25	0.45
α_s (m^2/g)	16.8	36.8	180	406
k_{app} (min^{-1})	0.12	0.22	0.33	0.73
k_{obs} ($L \cdot g_{pd}^{-1} \cdot min^{-1}$)	112	212	315	692
k_{SA} (L min^{-1} m^{-2})	6.7	5.8	1.8	1.7
initial TOF (mol TCE·mol^{-1} Pd·min^{-1})	150	134	50	62

To further examine the surface catalytic activity of the Pd nanoparticles for TCE hydrodechlorination, turnover frequency (TOF) is calculated. TOF is defined as moles of TCE degraded per mole of surface Pd atom per min. The initial turnover frequency (TOF_{init}) can be calculated via

$$TOF_{init} = -\left(\frac{d[TCE]}{dt}\right)_{t=0}\left(\frac{1}{[Pd]D_{Pd}}\right) \quad (4)$$

where D_{Pd} is the ratio of the number of surface Pd atoms to the number of total Pd atoms of a nanoparticle and [Pd] is the molar concentration of the Pd nanoparticles in the reaction system. To estimate the number of surface Pd atoms, the model of full-shell nanoparticles developed by Benfield is employed.[26] This model was employed by a number of researchers to figure out the specific surface area of small Pd nanoparticles. For example, Li et al.[12] applied it to PVP-stabilized Pd nanoparticles of 2.4 to 4.7 nm. Assuming that the CMC-Pd nanoparticles are cuboctahedral in shape with a cubic close packed (fcc) structure over this size range, a Pd nanoparticle is treated as a central atom surrounded by concentric shells of atoms. If the single central atom is counted as the core, a particle of m complete shells has edge length ($m + 1$) atoms. Starting at the single core atom ($m = 0$), the mth shell contains ($10m^2 + 2$) atoms. Further, the total number of atoms in a complete cluster sums to $(1/3)(2m + 1)(5m^2 + 5m + 3)$, which corresponds to the well-known series of 13, 55, 147, ... With the Benfield's model, the total number of atoms, the number of surface atoms, and D_{Pd} for various sizes of the CMC-Pd nanoparticles are obtained and listed in Table 1. Here, the radius of a Pd atom is considered 0.138 nm.[27] On the basis of the total number of atoms for a given CMC-Pd nanoparticle, the surface area per gram of the Pd nanoparticles (i.e., α_s) can be obtained (see Supporting Information for details). On the basis of the D_{Pd} values, the values of TOF_{init} are calculated via eq 4 and are given in Table 1.

On the basis of the TOF_{init} values in Table 1, the surface-based catalytic activity of Pd nanoparticles follows the order

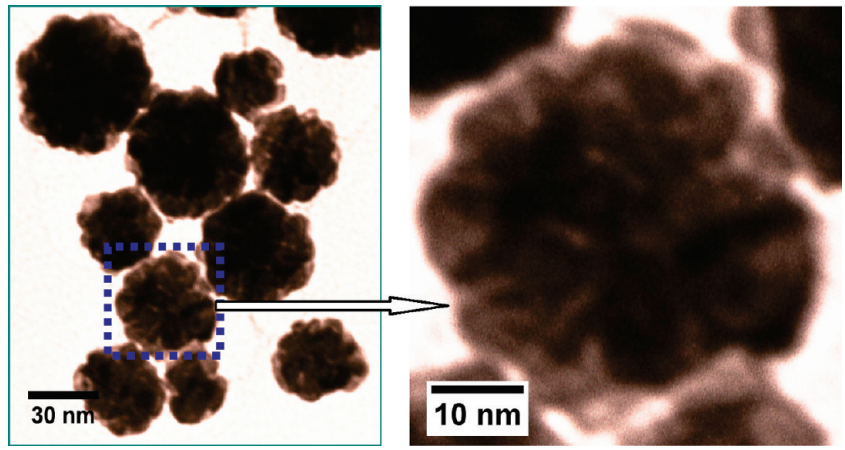

Figure 6. High-magnification TEM images of CMC-Pd nanoparticles synthesized at 50 °C. A TEM image at a reduced magnification is given in Figure S2 (Supporting Information).

of CMC-Pd (95 °C, 3.6 nm) > CMC-Pd (80 °C, 6.5 nm) < CMC-Pd (50 °C, 26 nm) < CMC-Pd (22 °C, 55 nm). The TOF_{init} value decreased from 62 mol TCE·mol^{-1} Pd·min^{-1} to 50 mol TCE·mol^{-1} Pd·min^{-1} as the particle size increased from 3.6 to 6.5 nm, while the k_{SA} values remained about the same. The greater TOF_{init} value for smaller particles is attributed to their greater fractions of active sites (edge and vertex atoms) on the Pd surface for TCE hydrodechlorination. However, when the particle size further increased from 6.5 to 55 nm as the synthesizing temperature decreased from 80 to 22 °C, the calculated TOF_{init} value increased by a factor of 2.7. This seemingly counterintuitive phenomenon can be attributed to the elevated underestimation of the reactive surface area for larger Pd nanoparticles with the Benfield's model. It is plausible that, for larger particles, the Pd atomic clusters are bound less tightly than for smaller particles. As a result, larger particles contain greater fractions of intraparticle pores and internal surface areas, which are not considered by the Benfield's model. This underestimation in surface area (and thus, the surface atoms) leads to underestimation of the D_{Pd} value, resulting in an overestimation of TOF_{init} for the larger particles. Figure 6 presents a high-magnification TEM image of the CMC-Pd nanoparticles synthesized at 50 °C. It is evident from the images that the nanoparticles are composed of smaller Pd clusters with uneven rough surfaces, suggesting that the nanoparticles are at least partially porous. The enlarged discrepancy between the model-calculated surface area and actual surface area for larger particles can also be revealed by comparing model-predicted surface area with reported Brunauer−Emmett−Teller (BET) measurements. For example, for the 55 nm particles, the Benfield's model would predict a surface area of only 16.8 m^2 g^{-1}. This number is a clear underestimation because it is even smaller than the BET surface area of 20−30 m^2/g generally reported for micrometer-scale metal particles,[9,10] which further indicates the existence of more intraparticle surface area for larger particles.

Compared to CMC-Pd synthesized using the conventional method (i.e., $NaBH_4$ reduction) ($D = 2.4 \pm 0.5$ nm; $k_{obs} = 731$ L g^{-1} min^{-1}; $TOF_{init} = 52$ L g^{-1} min^{-1}),[11] our "green" synthesized CMC-Pd nanoparticles ($D = 3.6 \pm 0.5$ nm; $k_{obs} = 692$ L g^{-1} min^{-1}; $TOF_{init} = 62$ L g^{-1} min^{-1}) are slightly larger but offer a comparable reaction rate and even greater surface catalytic reactivity under otherwise identical conditions. As detailed mechanisms are yet to be investigated, it appears plausible that the molecules of boric acid resulting from Pd^{2+} reduction by $NaBH_4$ may be adsorbed on the Pd surface, rendering a fraction of the surface area unavailable for TCE hydrodechlorination.[28] Because no harmful byproducts are formed with ascorbic acid, the "green" synthesis method also eliminates the attachment of undesired byproduct on the particle surface (or reaction sites).

For environmental cleanup applications, the highly dispersible CMC-Pd nanoparticles can be easily delivered into deep aquifers to facilitate in situ destruction of TCE. Compared to monometallic ZVI, the Pd nanoparticles offer unparalleled reactivity[6,7] and, thus, can be more cost-effective. The nanoparticles also may be immobilized on a porous support such as MgO and silica gel and used for hydrodechlorination in flow or batch reactor as described by Nutt et al.[29]

Role of CMC. The presence of CMC not only resulted in smaller and more uniform nanoparticles but also greatly improved the reactivity of Pd on a per-unit mass basis. The specific surface area gain of Pd nanoparticles is most sensitive to particle size in the size range of 1−10 nm. For instance, the surface atoms account for ∼90% of total atoms for 1 nm Pd clusters, compared to only ∼13% for 10 nm particles.[30] Nonstabilized Pd particles aggregate rapidly into 83−250 nm clusters, which correspond to a specific surface area of only 1−3 m^2/g,[31] compared to 16.8−406 m^2/g when CMC was present (Table 1).

The CMC used in this study is a linear polysugar with molecular weight of 90 000. In the synthesis of CMC-stabilized Pd nanoparticles, the CMC molecules complex with Pd^{2+} to give the precursor CMC-Pd^{2+}. The complexation did not appear to hinder significantly the subsequent reduction of the Pd^{2+} possibly owing to the rather bulky and loose structure of the CMC molecules. Thus, the primary role of CMC lies in facilitating the subsequent nucleation and growth of the Pd nanoparticles.

Our prior Fourier transform IR (FT-IR) results indicated CMC molecules can strongly interact with the Pd nanoparticle surface primarily through both the carboxyl (COO^-) and hydroxyl (−OH) groups.[11] These interactions facilitate the sorption of CMC molecules to form a monolayer of CMC molecules on the surface of Pd nanoparticles, resulting in the enhanced electrostatic and steric stabilization of the Pd nanoparticles. During the nucleation period, the association of CMC and the nuclei seeds prevented agglomeration of the seeds, favoring formation of larger number of nanoparticles, and thus smaller nanoparticles. During the nucleation and growth, the attached CMC molecules not only greatly confines the diffusivity of the growth species but also acts as a diffusion barrier for the growth

species to be taken up by the primary particles. Such diffusion control favors formation of more uniform and spherical particles.[25] Thermodynamically, the presence of the CMC layer provided an added energy barrier to resist the interparticle attractive forces and particle aggregation, which is in accord with the DLVO (Derjaguin, Landau, Verwey, Overbeek) theory. Note that, as two CMC-coated particles get closer, both electrostatic repulsion and steric hindrance (associated with osmotic pressure) become progressively pronounced.

The role of CMC is even more critical at elevated temperatures. This is because both collision energy and diffusion rate of the growth species are enhanced at higher temperatures, thereby favoring particle aggregation. Andreescu et al. reported that nonstabilized Au particles form unstable Au sols at temperatures above 55 °C due to the increased kinetic energy of the particles, which was able to overcome the energy barrier resulting from the electrostatic stabilization of Au particles.[32] In this present study, the coated CMC not only diminishes the kinetic energy but serves as diffusion barrier that warrants diffusion-controlled growth of Pd nanoparticles, resulting in the highly stable and narrowly distributed Pd nanoparticles at 95 °C. Considering the possibly greater hydrolysis of CMC molecules at elevated temperatures, such a barrier effect can be greater at higher temperatures because the broken-down CMC molecules may form a denser layer on the particle surface, which also favors diffusion-controlled growth. Furthermore, the conformation and CMC−CMC interactions may be altered at elevated temperatures. However, little is known in this aspect.

While the CMC layer greatly diminishes the kinetic energy and the mass transfer rate of the Pd nanoparticles, it may also inhibit surface reactivity as indicated by the decrease in the surface-area normalized rate constant (k_{SA}) as temperature increases (Table 1). However, the CMC layer does not appear to constitute a formidable barrier for the mass transfer and degradation of TCE. To the minimum, the kinetic barrier effect is far overwhelmed by the dramatic gain in the specific surface area and the overall reactivity as evidenced from the degradation data. This is attributed to the linear structure and larger molecular size of CMC molecules and their great effectiveness in particle stabilization. The k_{obs} value (692 L g^{-1} min^{-1}) for CMC-Pd is orders of magnitude greater than reported values. For instance, when nonstabilized Pd was used, the k_{obs} values ranged from 0.42 for Pd Black,[17] 0.64 for Pd/Al,[16] to 12.2 L g^{-1} min^{-1} for Pd/Al_2O_3.[16] CMC-Pd is also much more reactive than Pd nanoparticles that are stabilized by other stabilizers. For example, based on the k_{obs} values, it is 4.6 times more reactive than β-D-glucose stabilized Pd nanoparticles (mean size = 4.3 nm),[11] and 11 times more reactive than PVP-stabilized Pd nanoparticles (mean size = 6.1 nm).[17]

Conclusions

We demonstrate, for the first time, a "green" synthesis method for preparing highly reactive Pd nanoparticles. The nanoparticles are stable and comparable in reactivity to those prepared with the conventional borohydride reduction method. However, the use of environmentally benign and renewable materials (ascorbic acid and CMC) as the reducing and stabilizing agents offers the advantage of much reduced environmental impacts. The method may also provide a facile approach to synthesize other stabilized metallic (e.g., Au and Pt) nanoparticles, which hold the potential for various catalytic and optical applications. Furthermore, the nearly monodisperse nanoparticles obtained from this method can be used as seed particles for size-controlled growth of metal nanoparticles and for tunable construction of nanoparticle arrays that exhibit collective properties of individual nanoparticles.

Acknowledgment

The authors gratefully acknowledge the financial supports of a U.S. EPA STAR grant (GR832373), an Alabama Agricultural Initiative Grant, and an AAES Hatch/Multistate grant.

Supporting Information Available: Shown are digital images of Pd nanoparticle suspensions obtained at various temperatures and a magnified TEM image of CMC-Pd nanoparticles. In addition, details on the calculation of specific surface area of Pd nanoparticle based on the Benfield's model are presented. This information is available free of charge via the Internet at http://pubs.acs.org.

Literature Cited

(1) Cushing, B. L.; Kolesnichenko, V. L.; O'Connor, C. J. Recent Advances in the Liquid-Phase Syntheses of Inorganic Nanoparticles. *Chem. Rev.* **2004**, *104*, 3893.

(2) Schulz, J.; Roucoux, A.; Patin, H. Reduced transition metal colloids: A novel family of reusable catalysts. *Chem. Rev.* **2002**, *102*, 3757.

(3) Raveendran, P.; Fu, J.; Wallen, S. L. Completely "Green" Synthesis and Stabilization of Metal Nanoparticles. *J. Am. Chem. Soc.* **2003**, *125*, 13940.

(4) Dahl, J. A.; Maddux, B. L. S.; Hutchison, J. E. Toward Greener Nanosynthesis. *Chem. Rev.* **2007**, *107*, 2228.

(5) Anastas, P. T.; Warner, J. C. *Green Chemistry:Theory and Practice*; Oxford University Press: New York, 1998.

(6) He, F.; Zhao, D. Preparation and characterization of a new class of starch-stabilized bimetallic nanoparticles for degradation of chlorinated hydrocarbons in water. *Environ. Sci. Technol.* **2005**, *39*, 3314.

(7) He, F.; Zhao, D.; Liu, J.; Roberts, C. B. Stabilization of Fe-Pd nanoparticles with sodium carboxymethyl cellulose for enhanced transport and dechlorination of trichloroethylene in soil and groundwater. *Ind. Eng. Chem. Res.* **2007**, *46*, 29.

(8) Saleh, N.; Phenrat, T.; Sirk, K.; Dufour, B.; Ok, J.; Sarbu, T.; Matyjaszewski, K.; Tilton, R. D.; Lowry, G. V. Adsorbed Triblock Copolymers Deliver Reactive Iron Nanoparticles to the Oil/Water Interface. *Nano Lett.* **2005**, *5*, 2489.

(9) Schrick, B.; Hydutsky, B. W.; Blough, J. L.; Mallouk, T. E. Delivery vehicles for zerovalent metal nanoparticles in soil and groundwater. *Chem. Mater.* **2004**, *16*, 2187.

(10) Wang, C. B.; Zhang, W. X. Synthesizing Nanoscale Iron Particles for Rapid and Complete Dechlorination of TCE and PCBs. *Environ. Sci. Technol.* **1997**, *31*, 2154.

(11) Liu, J.; He, F.; Durham, E.; Zhao, D.; Roberts, C. B. Polysugar-Stabilized Pd Nanoparticles Exhibiting High Catalytic Activities for Hydrodechlorination of Environmentally Deleterious Trichloroethylene. *Langmuir* **2008**, *24*, 328.

(12) Li, Y.; Boone, E.; El-Sayed, M. A. Size effects of PVP-Pd nanoparticles on the catalytic Suzuki reactions in aqueous solution. *Langmuir* **2002**, *18*, 4921.

(13) Liou, Y. H.; Lo, S. L.; Lin, C. J. Size effect in reactivity of copper nanoparticles to carbon tetrachloride degradation. *Water Res.* **2007**, *41*, 1705.

(14) Sun, Y.; Zhang, L.; Zhou, H.; Zhu, Y.; Sutter, E.; Ji, Y.; Rafailovich, M. H.; Sokolov, J. C. Seedless and templateless synthesis of rectangular palladium nanoparticles. *Chem. Mater.* **2007**, *19*, 2065.

(15) Agency for Toxic Substance and Disease Registry. U.S. Department of Health and Human Service. ToxFAQ for Trichloroethylene. http://www.atsdr.cdc.gov/tfacts19.html.

(16) Lowry, G. V.; Reinhard, M. Hydrodehalogenation of 1- to 3-carbon halogenated organic compounds in water using palladium catalyst and hydrogen gas. *Environ. Sci. Technol.* **1999**, *33*, 1905.

(17) Nutt, M. O.; Hughes, J. B.; Wong, M. S. Designing Pd-on-Au Bimetallic Nanoparticle Catalysts for Trichloroethene Hydrodechlorination. *Environ. Sci. Technol.* **2005**, *39*, 1346.

(18) Nuffield, E. W. *X-ray Diffraction Methods*; Wiley: New York, 1966.

(19) Kennedy, J. F. *Cellulose and its derivatives: Chemistry, biochemistry, and applications*; Halsted Press: New York, 1985.

(20) Gilbert, R. D. *Cellulosic Polymers, Blends, and Composites*; Hanser/Gardner Publications: Cincinnati, OH, 1994.

(21) Fasman, G. D. *CRC Handbook of Biochemistry and Molecular Biology*; CRC Press: Cleveland, OH, 1976.

(22) He, F.; Zhao, D. Manipulating the size and dispersibility of zerovalent iron nanoparticles by use of carboxymethyl cellulose stabilizers. *Environ. Sci. Technol.* **2007**, *41*, 6216.

(23) Shimmin, R. G.; Schoch, A. B.; Barun, P. V. Polymer size and concentration effects on the size of gold nanoparticles capped by polymeric thiols. *Langmuir* **2004**, *20*, 5613.

(24) Shen, J. Y.; Li, Z. Y.; Yan, Q. J.; Chen, Y. Reactions of bivalent metal ions with borohydride in aqueous solution for the preparation ultrafine amorphous alloy particles. *J. Phys. Chem.* **1993**, *97*, 8504.

(25) Cao, G. Z. *Nanostructures and Nanomaterials: Synthesis, Properties and Applications*; Imperial College Press: London, U.K., 2004.

(26) Benfield, R. E. Mean coordination numbers and the non-metal−metal transition in clusters. *J. Chem. Soc., Faraday Trans.* **1992**, *88*, 1107.

(27) Lide, D. R. *CRC Handbook of Chemistry and Physics*, 75th ed.; CRC Press: Boca Raton, FL, 1994.

(28) Zhao, S. Y.; Chen, S. H.; Wang, S. Y.; Li, D. G.; Ma, H. Y. Preparation, Phase Transfer, and Self-Assembled Monolayers of Cubic Pt Nanoparticles. *Langmuir* **2002**, *18*, 3315.

(29) Nutt, M. O.; Heck, K. N.; Alvarez, P.; Wong, M. S. Improved Pd-on-Au bimetallic nanoparticle catalysts for aqueous-phase trichloroethene hydrodechlorination. *Appl. Catal., B* **2006**, *69*, 115.

(30) Nutzenadel, C.; Zuttel, A.; Chartouni, D.; Schmid, G.; Schlapbach, L. Critical size and surface effect of the hydrogen interaction of palladium clusters. *Eur. Phys. J. D* **2000**, *8*, 245.

(31) American Elements, Palladium Nanoparticles, http://www.americanelements.com/pdnp.html; Accessed in May 2009.

(32) Andreescu, D.; Sau, T. K.; Goia, D. V. Stabilizer-free nanosized gold sols. *J. Colloid Interface Sci.* **2006**, *298*, 742.

Received for review December 19, 2008
Revised manuscript received May 12, 2009
Accepted June 1, 2009

IE801962F